Chemical Engineering Journal 527 (2026) 171884

Contents lists available at ScienceDirect

Chemical Engineering Journal

journal homepage: www.elsevier.com/locate/cej

Ultra-thin Cr_2C MXene/polyaniline modified epoxy film for superior long-term corrosion protection

Abdulmajeed Al Askar [a,b], Faris Hamdi [c], Ali Altaee [a,*], Armaghan Moghaddam [d], Hossein Ali Khonakdar [d,*]

[a] Centre for Green Technology, School of Civil and Environmental Engineering, University of Technology Sydney, 15 Broadway, NSW, 2007, Australia
[b] Department of Chemical Engineering, College of Engineering and Computer Sciences, Jazan University, Jazan, 45142, Saudi Arabia
[c] Department of Civil and Architectural Engineering, College of Engineering and Computer Sciences, Jazan University, Jazan, 45142, Saudi Arabia
[d] Faculty of Polymer Processing, Iran Polymer and Petrochemical Institute (IPPI), Tehran, 14965-115, Iran

ARTICLE INFO

Keywords:
Cr_2C MXene
Polyaniline (PANI)
Epoxy coating
Corrosion resistance
Passivation

ABSTRACT

Corrosion is a significant and costly issue for engineering industries. This study describes an anticorrosion coating based on the chromium carbide MXene (Cr_2CT_x) and polyaniline (PANI) in epoxy-polyamide matrix. The hybrid system was prepared by in-situ oxidative polymerization of aniline in the presence of few-layer Cr_2CT_x, which was dispersed in epoxy and cured with polyamide. XRD, FTIR spectroscopy, and SEM/EDS analyses demonstrated the successful combination of PANI and Cr_2CT_x nanosheets with the epoxy matrix, driven by favourable compatibility. Favourable hydrophobicity was also observed according to contact angle studies. Electrochemical studies were carried out in a 3.5 wt% NaCl solution for 60 days on an ultra-thin 10 ± 2 μm film, indicating the significantly better performance of 0.5 wt% Cr_2CT_x + 0.3 wt% PANI/epoxy coating. In this composite, the more stable OCP, a significant decrease of corrosion current density by 3.57 orders of magnitude ($\sim 3.73 \times 10^3$ fold), and a lower corrosion rate of 4.91×10^{-6} mm.year^{-1} in comparison with neat epoxy (0.006 mm.year^{-1}) and bare steel (0.018 mm·year^{-1}) was achieved. The protection efficiency of the coating reached ~99.97 %, demonstrating a performance improvement of more than three orders of magnitude relative to neat epoxy. EIS fitting revealed high impedance, coating, and charge transfer resistance, and multi-time-constant protection mechanisms, while the surface examination showed fewer cracks and corrosion defects for the hybrid film. Accordingly, the highly conductive PANI and lamellar Cr_2CT_x MXene can offer long-term corrosion resistance, making Cr_2CT_x-PANI/epoxy composite a promising candidate for advanced protective coatings in chloride environments.

1. Introduction

The corrosion of carbon steel in marine, industrial, and infrastructural settings poses significant concerns for society in terms of both safety and economic implications. Epoxy-based organic coatings are one of the most common anticorrosion protection systems, due to their excellent adhesion, mechanical and chemical resistance to many environmental conditions, including chloride-induced corrosion. However, most epoxy coatings have inherent weaknesses, including microstructural defects, water penetration through epoxy films, and limited mechanical strength. These result in the ultimate failure of the coating in long-term immersion and aggressive environmental conditions [1].

As such, extensive research and development work have been devoted to improving the barrier, mechanical, and electrochemical performance of organic coatings. In particular, using nanofillers such as two-dimensional (2D) materials has been shown to be very promising for the enhancement of epoxy coatings [2]. MXenes are a class of 2D transition metal carbides and nitrides with a general formula of $M_{n+1}X_nT_x$, where M represents an early transition metal, X is carbon and/or nitrogen, and T_x is surface functional groups. MXenes are commonly synthesized by the selective etching of the A-element layer from layered MAX phases [3]. These materials possess unique features, such as surface functionality, electrical conductivity, and a high aspect ratio, rendering them highly useful for polymer-based coatings.

Extensive works were conducted to implement titanium-based MXenes (e.g., $Ti_3C_2T_x$) into corrosion coatings as reinforcement

* Corresponding authors.
E-mail addresses: ali.altaee@uts.edu.au (A. Altaee), hakhonakdar@gmail.com (H.A. Khonakdar).

https://doi.org/10.1016/j.cej.2025.171884
Received 14 September 2025; Received in revised form 11 December 2025; Accepted 12 December 2025
Available online 15 December 2025

agents. One of the main concerns with titanium-based MXenes is that they become oxidized rapidly when exposed to ambient and aqueous environments [4], and hence, more attention was directed to chromium-based MXenes, such as Cr_2CT_x, owing to the lower affinity of Cr to O than Ti [5]. Ning et al. have shown that the controlled synthesis of Cr_2C MXene can result in ultrathin nanosheets that have better oxidation resistance, and, due to their high aspect ratio, they can be distributed in an epoxy matrix to form a dense network of tortuous paths that can effectively hinder the diffusion of corrosive species.

Intrinsically conducting polymers (ICPs), such as polyaniline (PANI), have also been explored as functional additives for anticorrosion coatings due to their redox reversibility, environmental stability, and the ability to drive the passivation of metal surfaces through oxide layer formation. In addition, because they are electrochemically active, they can have longer-term electrochemical activity than conventional inhibitors, which are likely to leach over time. PANI also has the potential to tune the interfacial redox environment, suppressing corrosion initiation and promoting surface healing [6–9].

To bring together the barrier and electrochemical stabilization effects, Cr_2CT_x MXene and PANI were hybridized in an epoxy matrix. The combination of both these additives into an epoxy coating is a new composite strategy, as it combines both passive and active protection schemes. On one hand, MXene sheets create nearly impermeable physical layers that act as substantial diffusion barriers to aggressive ions, while strengthening the coating. PANI, on the other hand, is capable of electrochemically stabilizing the steel electrolyte interface. The overall benefit of using MXene and PANI is the enhancement of the coating lifetime, especially in thin-film coatings where the efficiency of the added filler is critical, as well as the interfacial adhesion strength between the coating and the substrate.

While MXene and PANI have both been reported to improve the corrosion resistance of epoxy coatings, their synergistic potential in hybrid coatings has not been previously realized, at least with Cr_2CT_x MXene. To date, most literature has focused on the $Ti_3C_2T_x$ MXene. In addition, PANI is either added as a doped or blended polymer phase, where optimization of its dispersion or synergistic effects with other nanomaterials has not been sufficiently considered. Therefore, this study examines whether the proven $Ti_3C_2T_x$-PANI synergy can be translated to Cr_2CT_x, representing the first investigation of such a hybrid system for corrosion protection. Finally, while the primary focus of research has been on thicker coatings (40–100 μm), the practical considerations of weight and precision applications often require the use of thinner films (~10 μm).

In this work, the corrosion resistance of a novel and environmentally stable ultra-thin-film (10 μm ± 2) epoxy-polyamide coating containing 0.5 wt% of a few-layer Cr_2CT_x MXene and 0.3 wt% PANI was investigated. The Cr_2CT_x MXene was synthesized under oxidation-controlled conditions to preserve the nanosheet integrity, while PANI was used as a conductive additive in the coating. The research questions are: i) what is the efficiency of a few-layer Cr_2CT_x-based coating for corrosion protection, and ii) is the ultra-thin film of Cr_2C-PANI coating strong enough to prevent metal corrosion? Accordingly, the new coating was applied to mild steel substrates, and its corrosion resistance was evaluated in a 3.5 wt% NaCl solution over 60 days. Electrochemical impedance spectroscopy (EIS), potentiodynamic polarization (PP), and open-circuit potential (OCP) measurements were used to probe the time-dependent evolution of the coating's protective properties. Pure epoxy-coated steel and bare steel samples were also used as benchmark samples. Corrosion behaviour, barrier properties, degradation kinetics, and interfacial properties were compared. This work provides further understanding of the potential of MXene-polymer nanocomposites for anticorrosion applications and, in particular, a strategy that uses ultra-thin, environmentally stable coatings for long-term stabilization without reliance on conventional, leachable inhibitors.

2. Materials and methods

2.1. Materials

Carbon steel panels (QLCXC-35-K, 76 mm × 127 mm × 0.8 mm) were purchased from Thermoline Scientific Pty Ltd. (Australia). Polyamide curing agent (GF04392) was obtained from GLPBio Technology Inc. (USA). Cr_2C MXene powder (>95 % purity, Cat. No. MX-CZ-193) was purchased from Chemazone Inc. (Canada). Aniline monomer (≥99.5 %), ammonium persulfate (APS, ≥98 %), Bisphenol A diglycidyl ether, sodium chloride (NaCl), xylene, n-butanol, and dimethyl sulfoxide (DMSO, ≥99.9 %) were all purchased from Sigma-Aldrich (Merck Life Science Pty Ltd., Australia). All the chemicals were used without further purification. Deionized water was used in all experiments.

2.2. Preparation of Cr_2CT_x-PANI composite and neat epoxy

Polyaniline was prepared in situ by the oxidative polymerization method. APS was used as an oxidant. Aniline monomer was added to 1 M hydrochloric acid and cooled at 0–5 °C in an ice bath. An appropriate stoichiometric amount of APS was slowly added to the aniline solution under vigorous stirring. The reaction mixture was allowed to stir for 6 h to complete the reaction. The resulting emeraldine salt form of PANI was filtered, washed with deionized water and ethanol to neutrality, and dried in a vacuum oven at 50 °C for 24 h.

The multilayered Cr_2CT_x MXene powder (ML-Cr_2CT_x) was used as received and was further delaminated to a few-layer nanosheets (FL-Cr_2CT_x) to facilitate its laminar dispersion in the composite matrix. Delamination of ML-Cr_2CT_x MXene was done by stirring overnight in DMSO, followed by sonication using a probe sonicator (20 kHz, 40 % amplitude) for an hour in an ice bath. The dispersion was centrifuged at 3500 rpm. The clear supernatant containing the exfoliated FL-Cr_2CT_x was separated and freeze-dried overnight. Nanocomposite dispersion was prepared by mixing 16 mg of delaminated FL-Cr_2CT_x MXene and 9 mg of dried PANI in a mixture of xylene (0.54 mL), n-butanol (0.32 mL), and acetone (0.21 mL). The amounts of FL-Cr_2CT_x and PANI correspond to 0.5 wt% and 0.3 wt%, respectively, on the total solid mass. The dispersion was sonicated using a probe sonicator for 30 min. Afterward, 1.25 g of bisphenol A-type epoxy resin was added to the mixture and stirred at 1000 rpm for 15 min. The solvent was allowed to evaporate partially by keeping the suspension in a fume hood for 15 min. Then, 1.86 g of polyamide curing agent was added to the reaction mixture and stirred gently at 500 rpm for 5–10 min to avoid entrapping air bubbles (Fig. 1).

The prepared composite was coated on both sides of the pre-treated carbon steel panels with an approximate dry film thickness of 10 μm ± 2 μm using a 15 μm spiral wire bar coater. The coated panels were flash-dried for 20 min in ambient conditions. Then, oven-curing was performed for 1.5 h at 60 °C, followed by post-curing for 72 h at room temperature (~22 °C). The neat epoxy coating was prepared using the same procedure, with the only difference being the absence of FL-Cr_2CT_x and PANI nanofillers. The prepared neat epoxy resin formulation was coated onto the carbon steel panels in the same way as the composite samples. The coating was cured thermally and in ambient conditions, following the same procedure used for composite samples. After coating and curing, the coated samples were visually inspected for any defects such as bubbles, cracks, or discontinuities on their surface and cross-section. Uniform coatings without any visible defects were used for further EIS, Tafel extrapolation, OCP monitoring, and physical characterization.

2.3. Characterizations of Cr_2CT_x-PANI composite and neat epoxy

The XRD patterns of Cr_2CT_x MXene before and after delamination, PANI, and the FL-Cr_2CT_x/PANI hybrid were obtained using an X-ray diffractometer (XRD, BRUKER D8 DISCOVER) with Cu Kα radiation,

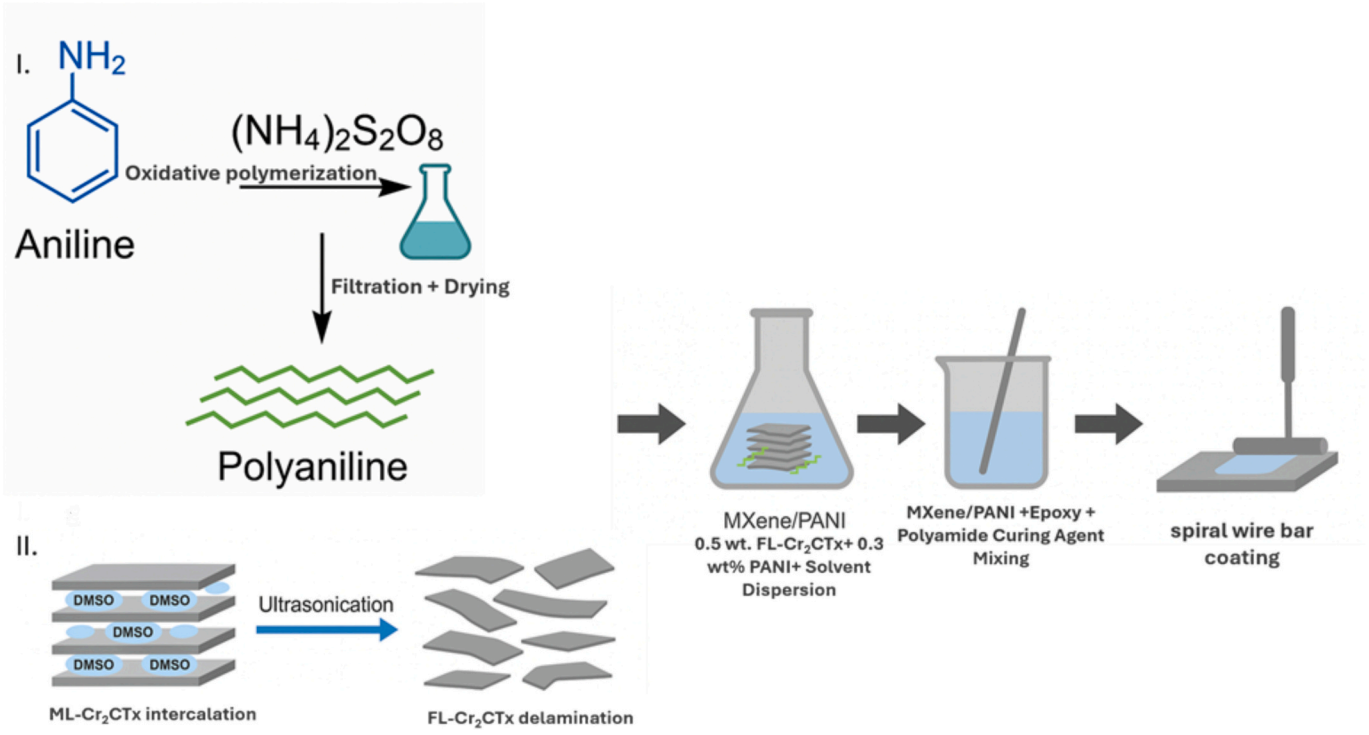

Fig. 1. Schematic illustration of the preparation and fabrication process for the Cr_2CT_x MXene-PANI/epoxy composite coating.

scanned over the 2θ range of 5–80° with a scan step of 0.04° (2θ). The surface morphologies and elemental composition of the samples were examined by scanning electron microscopy/Energy-dispersive X-ray spectroscopy (SEM/EDX, Zeiss Evo LS15) operated at an accelerating voltage of 15 kV after chromium sputtering. The chemical structures of neat epoxy, pure PANI, ML-Cr_2CT_x, and the FL-Cr_2CT_x/PANI hybrid, as well as the chemical structures of neat epoxy and the hybrid sample after the immersion test, were characterized by Fourier transform infrared spectroscopy (FTIR, Shimadzu MIRacle 10). The spectra were recorded in the range of 400–4000 cm^{-1} with a resolution of 4 cm^{-1}, and each spectrum was obtained by accumulating 45 scans. FTIR data were processed by baseline subtraction and Savitzky-Golay smoothing (OriginPro 2016). All spectra were analyzed in transmittance mode to preserve the original peak shapes and relative intensities. The surface wettability of the coatings was evaluated by static water contact angle (CA) measurements using a goniometer (CA, Biolin Attention Theta Lite).

The average stacking coherence length along the c-axis of FL-Cr_2CT_x was estimated mathematically using Bragg's law and Scherrer's relation.

$$n\lambda = 2d_{hk\ell}.sin\theta \quad (1)$$

Where n is the diffraction order, λ is the X-ray wavelength (1.5406 Å for Cu Kα radiation), d_{hkl} is the interplanar spacing for the crystallographic plane indexed by (*hkl*), and θ is the Bragg angle, used to calculate the basal spacing of the Cr_2CT_x MXene. For layered carbides, the interlayer spacing was obtained using:

$$d_{00\ell} = C/\ell \quad (2)$$

Where *C* is the lattice parameter along the c-axis and ℓ is the order of the basal reflection.

The average stacking coherence length along the c-axis was estimated using the Scherrer relation:

$$L^C = K\lambda/(\beta cos\theta) \quad (3)$$

Where K is the shape factor, λ is the X-ray wavelength, β is the full width at half maximum (FWHM) of the (002) peak in radians, and θ is the Bragg angle; this is standard XRD practice for layered carbides [10].

2.4. Corrosion study

The corrosion protection performance of the coatings was characterized by immersion and electrochemical measurements. The immersion test was conducted in a 3.5 wt% NaCl solution for 60 days to reproduce marine environmental conditions. The exposed surfaces of the samples (bare steel, neat epoxy, and FL-Cr_2CT_x-PANI/epoxy) were inspected before and after immersion using SEM to observe the morphological changes.

The electrochemical measurements were performed by an EmStat4S HR electrochemical workstation (PalmSens, The Netherlands) attached to the coating evaluation cell. The conventional three-electrode system was used, where the coated steel samples acted as the working electrode (13.85 cm^2), the saturation calomel electrode (SCE) served as the reference electrode, and the counter electrode was a graphite rod. All measurements were conducted in a 3.5 wt% NaCl solution that was naturally aerated at room temperature. OCP was monitored for 10 min before any further testing to allow for stabilization. EIS measurements were then performed in the frequency range of 0.01 Hz to 100 kHz with a sinusoidal perturbation amplitude of 5 mV around OCP. The spectra were analyzed with the aid of equivalent circuit fitting in PSTrace software to extract the coating resistance, charge-transfer resistance, and other interfacial parameters.

After the immersion test, the PP measurements were carried out by scanning from −20 mV to +20 mV vs. OCP with a scan rate of 1 mV/s. The values of corrosion potential (E_{corr}), corrosion current density (I_{corr}), and corrosion rate were obtained by Tafel extrapolation. The combined immersion electrochemical approach was used to characterize the degradation mechanisms and corrosion protection efficiency of the coatings during the 60-day immersion period.

The constant phase element (*CPE*) was converted into a capacitance (Q_x) using Brug's formula:

$$Q_x = \left(CPE \bullet R^{1-n}\right)^{\frac{1}{n}} \quad (4)$$

Where R is the equivalent resistance, n is the *CPE* exponent, while both the PP and EIS-related coating efficiencies were calculated as follows:

$$\eta_{PP}(\%) = \left[1 - \frac{i_{corr.of\ coated\ steel}}{i_{corr.of\ the\ bare\ steel}}\right] \times 100 \quad (5)$$

Where i is the current density [2] and

$$\eta_{EIS}(\%) = \left[1 - \frac{R_t^{reference}}{R_t^{protected}}\right] \times 100 \quad (6)$$

where $R_t^{reference}$ is the total resistance of the referenced system and $R_t^{protected}$ is the total resistance of the protective coating [6].

3. Results and discussion

3.1. Analysis of Cr_2CT_x composite materials

Fig. 2 summarizes the structural characterization of the chromium-carbide MXene-based systems under consideration: ML-Cr_2CT_x, FL-Cr_2CT_x, PANI powder, and the FL- Cr_2CT_x-PANI/EP coating (0.3 wt% PANI +0.5 wt% Cr_2C in epoxy). The XRD and FTIR data are in tandem with literature-supported density functional theory (DFT) to identify the dominant termination state, basal ordering, and polymer-filler interactions that can modulate dispersion and composite quality.

Fig. 2A schematic diagram illustrates the selective etching of the MAX phase precursor Cr_2AlC to produce Cr_2CT_x MXene. The aluminium layers are removed, and the surface is terminated with functional groups (—O, -OH, —F). These chemical modifications lead to few- to multi-layered MXene sheets with very high surface activity. SEM micrograph of ML-Cr_2CT_x (Fig. 2B) shows stacked, accordion-like morphology (typical of etched MXenes), with open interlayer spacing that allows for further exfoliation and surface functionalization.

The FL- Cr_2CT_x diffractogram in Fig. 2C is readily resolved into a clean basal 00ℓ series: (002) at 13.95° 2θ, (004) at 26.55°, and (006) at 42.59°, from which we obtain $d_{002} = 6.345$ Å and c = 12.69 Å. The (002) reflection of FL- Cr_2CT_x shows FWHM ≈ 2.35 ± 0.04° (2θ), determined by Gaussian fit (OriginPro) with scan step 0.04° (2θ), for a Scherrer stacking coherence length along c of $L^c \approx 3.41$ nm and an average coherent stack size of ~5–6 layers ($N \approx L^c/d_{002}$). This 00ℓ sequence and contracted c-parameter are in line with literature reports of well-washed/dried, O-rich Cr_2CT_x, in which delamination suppresses non-

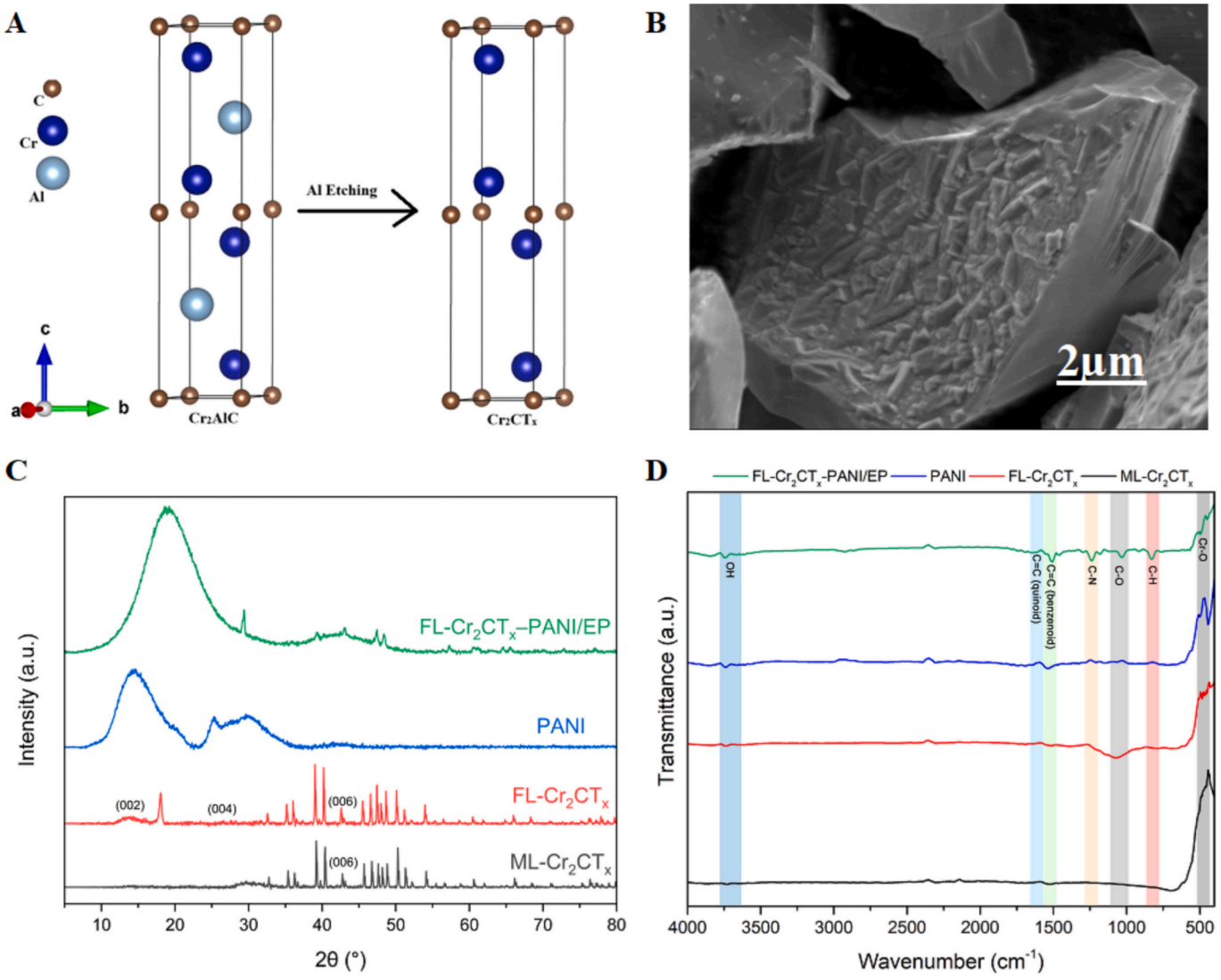

Fig. 2. Characterization of Cr_2C MXene and composites: (A) Etching schematic: $Cr_2AlC \rightarrow Cr_2CT_x$ (T_x = -O/-OH/-F), (B) SEM of ML-Cr_2CT_x MXene (scale: 2 µm), (C) XRD (Cu Kα): ML-Cr_2CT_x shows weak basal 00ℓ peaks; FL-Cr_2CT_x shows more intense basal 00ℓ peaks ((002) ≈ 13.9°, (004) ≈ 26.5°, (006) ≈ 42.7°); FL-Cr_2CT_x-PANI/EP displays a polymer halo with residual MXene basal signatures and (D) FTIR (4000–400 cm^{-1}): MXene termination bands <1000 cm^{-1}; PANI features retained in FL-Cr_2CT_x-PANI/EP.

basal reflections to produce intense (002)/(004)/(006) near ~13.9°/26.5°/42° [11–15]. By contrast, immediately after etch/intercalation, some Cr_2CT_x preparations transiently exhibit a lower-angle (002) (~9–12°) associated with expanded galleries that collapse toward ~14° upon removal of water/volatile species [11]. These reference trajectories frame our own observations: the FL pattern evidences well-ordered, restacked few/mono domains, whereas the multilayered powder shows weaker/smeared higher-order basal reflections consistent with turbostratic disorder and less preferred orientation.

The ML-Cr_2CT_x diffractogram has a broad (002) near ~13–14° and weaker/smeared higher-order basal reflections, indicating turbostratic disorder and loss of interlayer registry. This progression is well known in the processing history of Cr_2CT_x: immediately after the etching, a lower-angle (002) emerges at ~9–12° (indicating expanded galleries), which contracts toward ~14° upon washing/drying as the intercalants and water are removed to leave behind stable O-terminated stacks (c ≈ 12.6–12.7 Å) [5,15]. Due to the substantial overlap potential at ~42° 2θ between the MAX precursor's (103) and the MXene (006) [11,15], a comprehensive exfoliation assessment should be based on the entire 00ℓ sequence and non-basal suppression, rather than a single line.

Finally, some minor non-basal features appear outside the 00ℓ series (for instance, the occasional sharp line near ~18° 2θ, and the like). However, these do not index to Cr_2CT_x 00ℓ reflections and are attributed to trace crystalline residues or mounting artefacts; thus, such features were excluded from lattice analysis. In general, in evaluating exfoliation, it is advised against placing too much emphasis near ~42° 2θ, where there can be some MAX (103) overlap with MXene (006); hence, the complete 00ℓ sequence and non-basal suppression are preferred over a single line.

The diffractogram of the FL-Cr_2CT_x-PANI/EP coating in Fig. 2C is predictably dominated by the polymeric matrix (amorphous halo in the ~18–30° window) at these 3 wt% total fillers. Nevertheless, faint basal cues can persist most often on a shoulder near ~26.5°, attributable to the (004) of well-oriented platelets. To avoid mis-assignments, PANI powder is plotted as a reference: its broad, low-crystallinity bands near ~20–21° and ~ 25–26° (commonly indexed to PANI (020)/(200)) provide an explicit delimiter between polymer and MXene contributions in the composite pattern [6–9]. In short, XRD confirms that our FL-Cr_2CT_x preparation retains lamellar order consistent with oxygen-rich surfaces, while the coating pattern is matrix-dominated with residual MXene signatures, exactly the behaviour expected at low loading.

DFT analyses, specific to Cr-based MXenes, show that while -F/-OH/-O terminations can form during the etching, O-terminated surfaces are energetically favoured after washing/drying; simulated patterns for O-terminated Cr_2CT_x reproduce the experimentally observed (002) position close to the MAX-like spacing near ~14° [11,15]. The close agreement between our measured c-parameter (12.69 Å) and these O-terminated models supports the assignment that the FL-Cr_2CT_x examined here is predominantly O-terminated at the time of XRD/FTIR acquisition (Fig. 2C & 1D). This termination state is not just a structural detail; rather, it controls polarity, hydration, and interfacial chemistry in the composite.

FTIR spectra (Fig. 2D) provide further evidence for the O-rich surface chemistry and interlayer hydration of FL-Cr_2CT_x MXene. Characteristic absorptions of the Cr—O triplet are evident in the low-wavenumber region (~647, 608, and 462 cm^{-1}), while the broad O—H stretching band centred near ~3600 cm^{-1} and the H-O-H bending mode at ~1630 cm^{-1} also underscore the prevalence of surface hydroxyl/oxo groups and adsorbed/interlayer water molecules, in line with prior reports for Cr_2CT_x MXenes [5]. A broad band centred near ~1080 cm^{-1} can be assigned to carbonate C—O stretching, originating from the adsorption of ambient CO_2 onto the hydroxylated MXene surface [11], a phenomenon frequently reported for O-terminated transition-metal carbides.

In the case of the PANI reference, the spectrum features the canonical signatures of the conducting polymer: benzenoid and quinoid ring stretching at ~1500–1515 and ~ 1580–1600 cm^{-1}, respectively; benzenoid C—N stretching at ~1290–1320 cm^{-1}; the polaron-associated band at ~1100–1150 cm^{-1}; and the para-substituted C—H out-of-plane deformation near ~820–830 cm^{-1} [6,7,9]. A magnified FTIR view below 1600 cm^{-1} is provided in Fig. S2 to clarify low-intensity peaks, and the results of FTIR for the neat epoxy sample are shown in Fig. S3. All of these polymer bands are preserved in the FL-Cr_2CT_x-PANI/EP hybrid and corresponding epoxy coating, consistent with the structural integrity of PANI after hybridization and curing. Nevertheless, their subtle shifts and relative intensity changes in the quinoid/benzenoid and polaron regions, along with the persistence of the hybrid specific Cr—O vibrations in the 560–600 cm^{-1} range are the evidence of interfacial interactions, which are likely related to hydrogen bonding and charge transfer processes between the amine/protonated amine groups (-NH/-NH^+) of PANI and the O-terminated Cr_2CT_x surfaces, in line with reported MXene-polymer synergistic effects in PANI composites [6,7,9].

The EDS spectra presented in Table S.3 show the compositional evolution from ML-Cr_2CT_x to O-terminated FL-Cr_2CT_x and ultimately to FL-Cr_2CT_x-PANI/EP. In the ML-Cr_2CT_x powder, the high intensity of Cr and C signals with a minor oxygen peak confirmed the existence of the metallic carbide structure with a limited surface oxidation state. The FL-Cr_2CT_x had a significantly higher oxygen and a slightly decreased chromium content, which indicated the successful termination of the surface with stable O-terminated groups. In the FL-Cr_2CT_x-PANI/EP, the EDS spectra showed a uniformly balanced carbon, oxygen, chromium, and nitrogen signals, which confirmed the homogenous co-dispersion of the FL-Cr_2CT_x nanosheets and PANI particles in the epoxy matrix. The intensity of the nitrogen peak confirmed the doping of PANI, the high intensity of oxygen, and the intermediate signal of chromium indicated a strong interface between O-terminated FL-Cr_2CT_x and polymer chains through Cr-O-N and Cr-O-C interactions. In general, as shown in Table S.3, the EDS spectra revealed that the FL-Cr_2CT_x-PANI/EP coating has uniformly dispersed O-terminated FL-Cr_2CT_x nanosheets and conductive PANI, which together establish a well-integrated hybrid network that improves the structural integrity, adhesion, and dual corrosion-protection mechanisms (barrier and redox-active effects). In effect, EDS analysis showed a steady increase in oxygen content after delamination, in agreement with the steady surface O-termination, instead of extensive structural oxidation. Both oxygen and chromium contents remained stable after incorporation into the epoxy matrix, implying no aggressive oxidation during processing.

Taken together, the convergent picture from Fig. 2 and Table S.3 suggests that O-terminated, lamellar FL-Cr_2CT_x underpins the processability and dispersion observed empirically. The O-rich surface increases polarity and hydrogen-bonding capacity, improving wetting with PANI and the epoxy/curative and promoting colloidal stability in pre-mix. The XRD shows that platelets retain basal order (00ℓ series) after delamination/restacking, and the FTIR and EDS confirm surface oxygen functionality with interlayer carbonate typical of Cr-based MXenes. These structural/chemical attributes are precisely those leveraged in the recent study of chromium-based MXenes as barrier nanosheets in corrosion-protection coatings, where oxidation control and termination chemistry dictate both dispersion and durability [5]. Accordingly, the superior dispersion of FL-Cr_2CT_x relative to ML-Cr_2CT_x pristine powder is attributed to its O-termination-dominated surface chemistry and reduced stacking disorder, a conclusion independently supported by our XRD metrics (c, FWHM, L_c) and FTIR fingerprints.

These structural features are directly relevant to corrosion protection. Well-ordered lamellae can create a more tortuous pathway that slows the entry of water and chloride ions in saline conditions, while the O-terminated surfaces help PANI and epoxy bond more effectively through hydrogen bonding and charge transfer. These effects improve dispersion, adhesion, and barrier stability synergistically, which explains the strong long-term electrochemical performance observed in this study [16].

3.2. Morphology, hydrophobicity, and visual investigation of Cr_2CT_x/PANI additive in epoxy coating

Fig. 3 (A1-H2) reports the SEM micrographs of the coatings and the steel substrate before and after immersion in 3.5 wt% NaCl solution. FL-Cr_2CT_x-PANI/EP hybrid, neat epoxy, and bare steel were compared to highlight the impact of the nanofiller system on coating compactness, film integrity, and interfacial protection. Fig. 3 (A1 & A2) shows direct morphological evidence of the stability imparted by the hybrid coating. Panel A1 (before immersion) indicates that the FL-Cr_2CT_x-PANI/EP surface was compact, homogeneous, and free of cracks and voids. This finding confirmed that the presence of nanoscale additives promoted the formation of an epoxy film (rather than loose agglomerates or clusters), following the processing steps outlined in the methods section. After 60 days of immersion (A2), the surface morphology remained relatively intact, with minor micro-roughening and isolated surface features, without heavy cracking or delamination. This outcome can be reasonably associated with the combined influence of the conductive PANI network and the structural features of FL-Cr_2CT_x nanosheets, which have been reported to act synergistically in related MXene-based coatings [7–9]. In combination, these components established a tortuous path for electrolyte diffusion and buffered charge transfer reactions at the coating-metal interface. It is also noted that similar synergistic effects have been previously reported for MXenes/conducting polymer hybrids, wherein coating morphology stabilization and the retardation of water ingress were obtained under aggressive environments [6–8].

In Fig. 3 (B1 & B2), the behaviour of neat epoxy coatings under the same conditions is compared. Before immersion (B1), the epoxy surface was smooth and free of defects. However, after 60 days (B2), the coating displays extensive cracking, blister caps, and surface roughening, which are typical signatures of water uptake, plasticization, and osmotic blister formation in conventional epoxy films [17–19]. These defects would provide a continuous transport channel for electrolyte transport and promote accelerated under-film corrosion and interfacial detachment. The difference in performance between the composite and neat coatings is particularly evident and highlights the limited durability of neat epoxy in the presence of chloride ions.

Cross-sectional SEM micrographs, Fig. 3 (C1-C3), were also collected to support the above observations further. The thickness of the FL-Cr_2CT_x-PANI/EP coating was confirmed to be ~10 ± 2 μm, as shown in cross-sectional SEM micrographs. The ultra-thin coating shows no diminished protection; in fact, the cross-sectional morphology remained consistent and uniform, with firm adherence to the substrate and no interfacial voids. Although the observations indicate good adhesion and a compact coating structure, mechanical evaluation will be necessary in future work to confirm these findings. After 60 days (C2 & C3), the hybrid coating also largely retained its compact morphology and adhesion, demonstrating that the interfacial region was not weakened by the immersion period and that the nanoscale additives inhibited delamination. The capacity of the composite system to deliver excellent corrosion resistance, even with a film thickness that was about 1/10 of the sample, highlights high-performance coatings, which may typically require ~100 μm to achieve a similar level of long-term performance [5]. The proposed hybrid structure exhibited durability even at ~10 ± 2

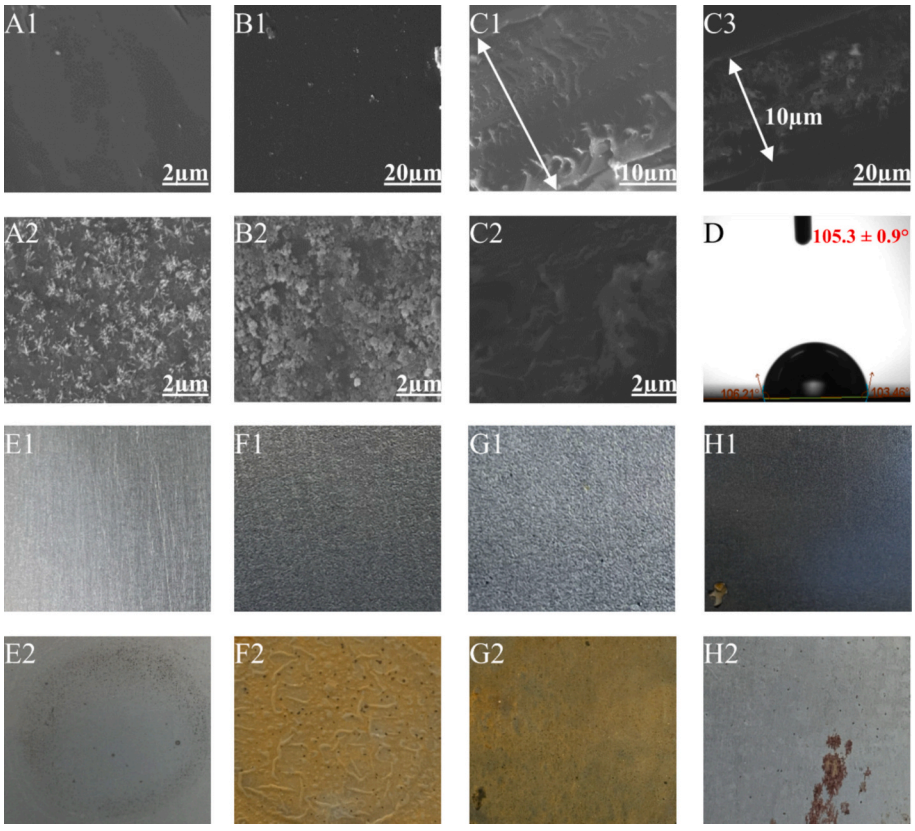

Fig. 3. SEM and surface analyses of the bare steel, neat epoxy, and FL-Cr_2CT_x-PANI/EP coatings before and after immersion in 3.5 wt% NaCl solution for 60 days: (A1, A2) SEM micrographs of the FL-Cr_2CT_x-PANI/EP coating before and after immersion, showing compactness and stability with only minor surface roughening, (B1, B2) SEM micrographs of the neat epoxy surface before and after immersion, revealing cracking and blistering after long-term exposure, (C1-C3) Cross-sectional SEM micrographs of the FL-Cr_2CT_x-PANI/EP coating (~10 μm ± 2), (D) Static water contact angle image, showing hydrophobicity of the FL-Cr_2CT_x-PANI/EP (~106°), (E1, E2) Photographs of bare steel before and after immersion, with severe pitting and oxide formation after 60 days, (F1, F2) Photographs of neat epoxy before and after immersion, displaying surface degradation and interfacial corrosion, (G1, G2) Photographs of FL-Cr_2CT_x-PANI/EP before and after immersion, showing intact morphology with only localized changes, and (H1,H2) Photographs of steel substrates beneath the coatings after 60 days, demonstrating severe corrosion under neat epoxy versus largely preserved metallic surface under the FL-Cr_2CT_x-PANI/EP.

μm due to its unique ability to provide tortuous ion-diffusion pathways (Cr_2CT_x nanosheets) and redox passivation (PANI) [5,7].

Fig. 3D reports water contact angle measurements for epoxy coatings, which provided further surface property evidence on wetting. In this case, the FL-Cr_2CT_x-PANI/EP coating exhibited a contact angle of 105.3 ± 0.9°. The resulting droplet profile was spherical and consistent with the hydrophobicity of the hybrid surface. Such water repellency will restrict electrolyte wetting and penetration, thereby improving protection. This result is in line with previous studies, which have shown that conductive polymer-MXene hybrids can significantly increase surface roughness and alter surface energy, producing a higher water repellency compared to conventional epoxy resins [5,7]. Given that the adsorption of water is a known trigger for epoxy failure, the hydrophobicity of the hybrid coating can be considered a key contributor to its long-term stability. The combination of low interfacial wettability and extended diffusion pathways results in a dual barrier mechanism that explains the superior electrochemical stability observed in OCP and EIS measurements.

Fig. 3E1 & E2 show the performance of an uncoated steel substrate tested under the same conditions as the FL-Cr_2CT_x-PANI/EP. Before immersion (E1), the substrate exhibited a clean and featureless metallic surface. However, after 60 days (E2), the steel exhibited widespread corrosion, as evidenced by the appearance of deep pits, roughened surfaces, and thick oxide deposits. These morphological features are consistent with the uncontrolled electrochemical activity of the steel surface in the chloride media and highlight the importance of protective coatings. Fig. 3F1 & F2 further demonstrate the behaviour of neat epoxy coatings after immersion. In this case, while the surface was visually intact before the test (F1), immersion in saline solution led to significant deterioration after 60 days (F2), which can be seen in the form of cracking and blistering of the coating surface.

In contrast, the FL-Cr_2CT_x-PANI/EP system, as shown in Fig. 3 (G1 & G2), shows a much more favourable behaviour. Before immersion (G1), the surface of the composite coating was smooth and free of defects. However, after immersion (G2), it retained much of its compactness, with only minor localized surface roughening without heavy delamination and extensive cracking. This stability is consistent with the superior barrier properties imparted by the hybrid filler system, despite the fact that it results from only a thin film with a thickness of ~10 μm. FL-Cr_2CT_x nanosheets may have created a physical labyrinth that obstructed and retarded ionic and molecular transport, while the PANI phase may have contributed by a mechanism of redox passivation at defect sites, promoting redox-related stabilization that further suppressed corrosion. However, this proposed synergistic mechanism requires further investigation to be conclusively established; nonetheless, the present results clearly demonstrate the strong corrosion protection performance of the coating. Finally, examination of the substrate beneath the coating layer after the immersion test, Fig. 3H1& 3H2, revealed a stark contrast in performance. In the case of neat epoxy (H2), the steel surface was severely corroded, as can be seen in the presence of a visible oxide layer and surface roughening. In contrast, the steel surface beneath the FL-Cr_2CT_x-PANI/EP coating remained much more intact, with only minor discoloration and negligible oxide accumulation, as shown in H1. These results demonstrate that the hybrid system was successful in providing effective under-film protection, isolating the substrate even after a challenge with chloride ions.

Overall, the above morphological results confirm that the FL-Cr_2CT_x-PANI/EP coating delivered significantly better durability and substrate protection than neat epoxy and bare steel. This advantage was realized with a dry coating thickness of ~10 ± 2 μm. The result is a testament to the material efficiency of the proposed hybrid system, as it is widely accepted that conventional epoxy coatings would require substantially thicker films of 20–100 μm to maintain long-term performance. Nevertheless, the combination of FL-Cr_2CT_x nanosheets and PANI enabled the formation of compact films, hydrophobicity, and interfacial passivation, which collectively provided robust and reliable protection at lower thicknesses. In addition to the scientific significance of the FL-Cr_2CT_x-PANI/EP hybrid, such performance has clear practical advantages in terms of reduced material use, lower cost of application, and improved sustainability.

3.3. Anticorrosion property of the Cr_2CT_x-PANI composite

3.3.1. Electrochemical characterizations

3.3.1.1. Open circuit potential (OCP) measurements. Bare steel presented the lowest and least stable potential values (−0.730 to −0.645 *V* vs. SCE) compared to the neat epoxy and FL-Cr_2CT_x-PANI/EP systems during the immersion test, while the neat epoxy experienced the most negative shift of OCP in the 3.5 wt% NaCl solution (Fig. 4A). The more noble OCP value of the neat epoxy coating (−0.356 *V* vs. SCE at day 0) compared to bare steel is consistent with reduced anodic activity relative to bare steel, although OCP alone does not confirm barrier performance [5]. A more noble OCP may result from either inhibited anodic dissolution or the development of an interfacial oxide layer; therefore, the OCP trend is evaluated together with EIS and polarization data to provide a reliable interpretation of the coating behaviour. However, a substantial and steady fluctuation and negative shift after day 14 revealed that the epoxy matrix might have been penetrated by electrolyte, leading to under-film interfacial corrosion [5]. The FL-Cr_2CT_x-PANI/EP coating, on the other hand, presented an average value of OCP from −0.44 to −0.23 V vs. SCE with much milder potential fluctuations during the first 14 days of immersion (Fig. 4A). The relatively stable OCP of the coating suggested that it was not as easy for the 3.5 wt% NaCl solution to cause the potential drop of the composite coating, most probably due to the barrier/passivation actions of FL-Cr_2CT_x-PANI. The layered exfoliated FL-Cr_2CT_x nanosheets acted as an effective tortuous diffusion channel barrier to corrosive ions, while the conductive PANI could facilitate the formation of a passivation layer on the coating substrate interface [6]. As shown in Fig. 4A, a slight negative shift started to occur after day 21 for the FL-Cr_2CT_x-PANI/EP coating. The OCP values remained more favourable than those of bare steel and were very close to the values measured for the neat epoxy coating, confirming effective corrosion protection. The results imply that although some degradation may occur, the barrier/passivation function still delays the loss of the coating's integrity to a certain extent, despite the low thickness of the coating. As previously reported, similar, more noble potentials were observed for FL-Cr_2CT_x-PANI/EP hybrids, where the conductive polymer passivation layer synergized with the 2D nanofillers' physical barrier [9]. Therefore, OCP measurement is a sensitive approach to monitor the early degradation stage of a coating system. The obtained results for all the samples during the immersion tests also suggested that the FL-Cr_2CT_x-PANI/EP coating system had a better long-term stability than the neat epoxy coating.

The FL-Cr_2CT_x nanosheets reduce ionic transport into the coating, while the PANI component can participate in reversible redox reactions that re-stabilize barrier properties, the effects of which distinguish the designed hybrid system from purely passive systems, where OCP stability is governed solely by physical barrier effects. Therefore, suppressing large potential drops during immersion reflects not only inhibited electrolyte penetration but also an electrochemically active interfacial stabilization mechanism.

3.3.1.2. Potentiodynamic polarization (PP). Table 1 and Fig. 4B summarize the PP data for the bare steel, pure epoxy, and the modified epoxy samples. The data for the bare steel shows the active dissolution of the substrate ($E_{corr} = -0.727$ *V* vs. SCE, $i_{corr} = 1.576 \times 10^{-6}$ A cm^{-2}, and a corrosion rate of 0.018 mm $year^{-1}$), while the neat epoxy coating shifted E_{corr} positively to −0.410 V and reduced the value of the i_{corr} to 5.031×10^{-7} A cm^{-2}. The obtained corrosion rate for the neat epoxy coating is 0.006 mm $year^{-1}$, which corresponds to a protection

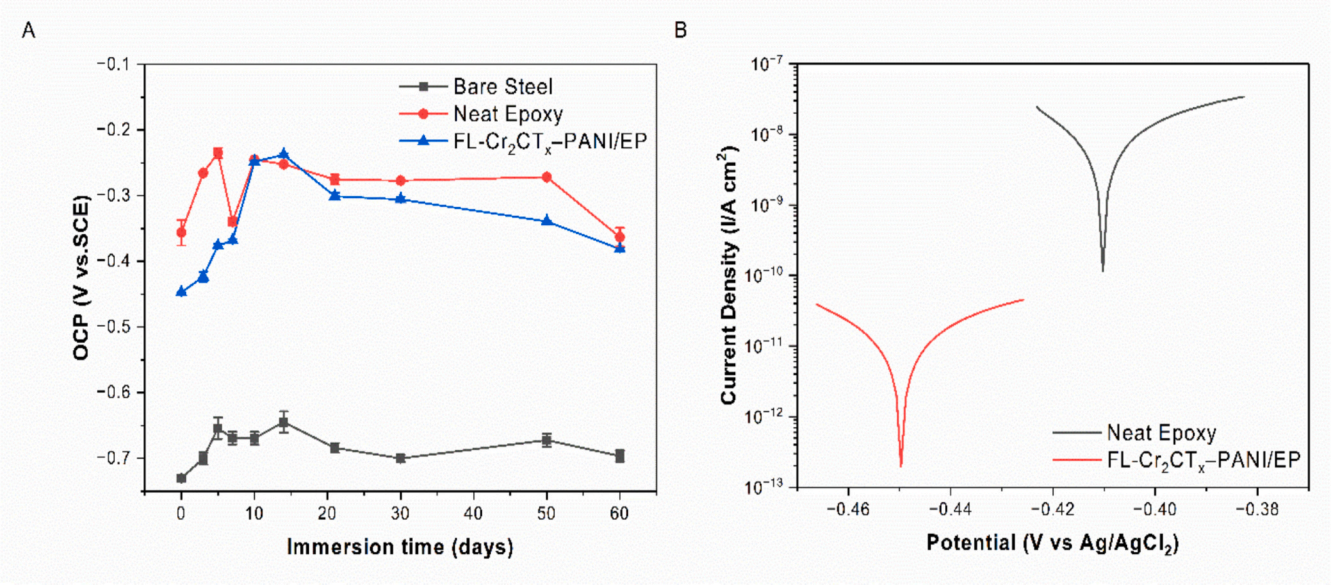

Fig. 4. Electrochemical performance of bare steel, neat epoxy, and FL-Cr_2CT_x-PANI/EP coatings in 3.5 wt% NaCl solution: (A) Open circuit potential (OCP) evolution for 60 days immersion, showing the values of the FL-Cr_2CT_x-PANI/EP coating compared to neat epoxy and bare steel, and (B) Potentiodynamic polarization (PP) before immersion in 3.5 wt% NaCl solution, where the FL-Cr_2CT_x-PANI/EP coating exhibits the highest polarization resistance, reflecting its superior long-term corrosion protection relative to neat epoxy and bare steel.

Table 1
The potentiodynamic parameters of bare steel, neat epoxy, and FL-Cr_2CT_x-PANI/EP composite.

Samples	E_{corr} vs. SCE (*V*)	i_{corr} (A/cm^2)	B_a (V/dec)	B_c (V/dec)	Corrosion Rate (mm/year)	η_{pp}(%)
Bare Steel	−0.727	1.576E-6	0.027	0.046	0.018	–
Neat Epoxy	−0.410	5.031E-7	0.171	0.081	0.006	68.08 %
Cr_2CT_x-PANI/EP	−0.450	4.226E-10	0.083	0.058	4.905E-6	99.97 %

efficiency (η_{pp}) of ~68 % when compared to the bare steel surface. This result could be ascribed to the barrier effect of the polymer matrix and its high compaction, which retards the diffusion of electrolyte species and oxygen molecules by the impermeability of 2D FL-Cr_2CT_x MXene, which elongates the path to the metal surface. FL-Cr_2CT_x-PANI/EP system featured an E_{corr} of −0.450 V and an ultralow i_{corr} of 4.226×10^{-10} A cm^{-2}, which can be attributed to the passivating effect of 2D FL-Cr_2CT_x nanosheets and PANI, as shown in their EIS trend (Fig. 7). The extremely low corrosion current corresponds to a corrosion rate of 4.905×10^{-6} mm $year^{-1}$ and η_{pp} of ~99.97 %. The unprecedented decrease in the corrosion current may be ascribed to the synergistic action of 2D nanosheets and PANI.

On one hand, 2D Cr_2CT_x nanosheets increase the tortuosity of the ion diffusion paths, which provides the coating with enhanced compactness [20]. On the other hand, the redox activity of PANI can cause anodic passivation of the steel [21]. These two effects, combined, produce a dramatic improvement in the anticorrosive properties of the polymer matrix. Indeed, the obtained corrosion rate for the FL-Cr_2CT_x-PANI/EP composite system is several orders of magnitude lower than that of the neat epoxy. The anticorrosion behaviour of FL-Cr_2CT_x-PANI/EP coatings is similar to/better than that of MXene-polymer systems and other conductive polymer composites [6–9]. The corrosion rate for these systems is much lower than that of unmodified epoxy, due to a combination of physical and active barriers that enable long-term corrosion protection in aggressive chloride media.

3.3.1.3. Electrochemical impedance spectroscopy (EIS). The fitting for all impedance data was carried out with the respective equivalent circuit, as mentioned in Fig. 5 (A-C) and Table S. 1 in the supplementary data. In addition, the EIS fitting data for the 0.5 wt% FL-Cr_2CT_x + 0.3 wt% PANI epoxy composite, as compared to neat epoxy and bare steel, are provided in Fig. 6 (A-F). For bare steel, a one R(QR) circuit was used for all the time points, since there was no coating and continuous exposure to electrolyte and metal as substrate. Neat epoxy, in general, showed a one-time-constant response. However, signs of Warburg diffusion behaviour from the early stage (day 3) were observed. Hence, the resistance, capacitance, and Warburg elements were used (R(QR)(W)). For the FL-Cr_2CT_x-PANI/EP system, a two-time-constant model (Fig. 5B) was

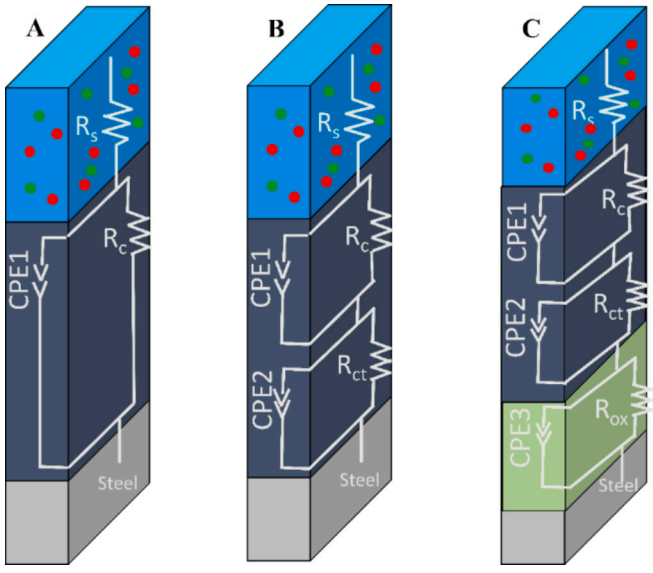

Fig. 5. (A-C) Equivalent electrical circuit models applied to describe the electrochemical responses.

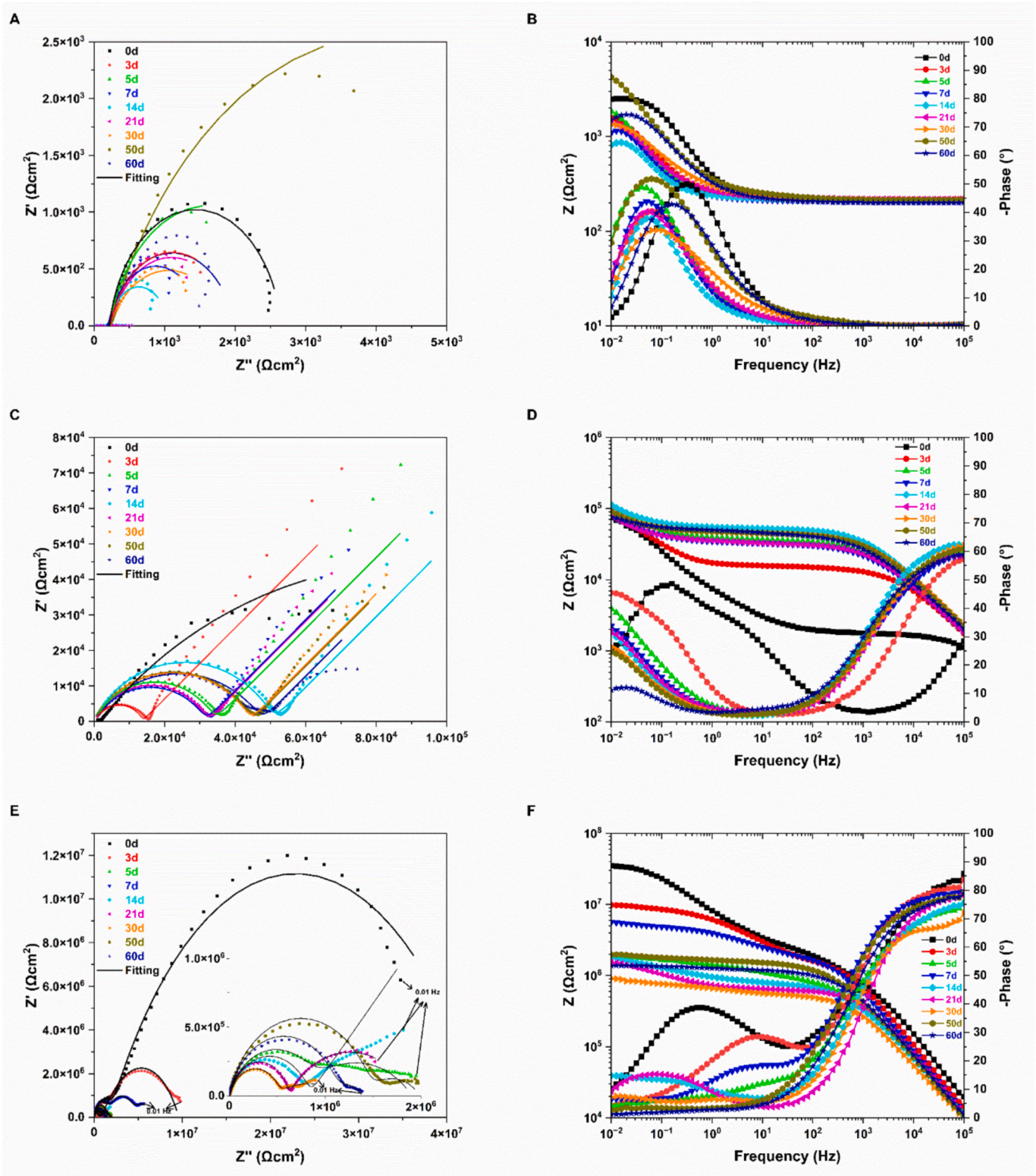

Fig. 6. Electrochemical impedance spectroscopy (EIS) results for bare steel, neat epoxy, and FL-Cr_2CT_x-PANI/EP coatings during 60 days immersion in 3.5 wt% NaCl solution: (A, B) Bare steel: Nyquist and Bode plots showing rapid degradation and low impedance, consistent with severe corrosion, (C, D) Neat epoxy: initial barrier response followed by progressive reduction in impedance and phase angle, indicating electrolyte penetration, blistering, and under-film corrosion, and (E, F) FL-Cr_2CT_x-PANI/EP: Nyquist and Bode plots reveal the highest impedance and most stable phase response throughout immersion, confirming superior long-term corrosion resistance due to the synergistic barrier effect of FL-Cr_2CT_x nanosheets and redox passivation from PANI.

required for most of the immersion time, except at the intermediate time point (Day 7), to account for the activity at the coating, interface, and oxide film (Fig. 5C), in addition to the Warburg element [R(Q[RW])] on Day 14, which required special attention for discussion of its corrosion behaviour and protection. The evolution of the equivalent circuit throughout immersion closely follows the physical stages of degradation observed in the impedance spectra. During Days 0–5, the R(QR)(QR) model captures both the coating barrier response and the interfacial charge-transfer process. The additional low-frequency arc observed on Day 7 indicates the development of a compact interfacial oxide layer, warranting the introduction of the third time constant (R_{ox}-Q_{ox}). At Day 14, the appearance of a diffusion tail demonstrates that electrolyte transport became rate-determining, which justified the use of the R(Q[RW]) model. Beyond this stage, the disappearance of the diffusion signature and the re-emergence of a two-semicircle response confirm that the system no longer exhibited diffusion-limited behaviour; therefore, the simplified two-time-constant model was reinstated to avoid over-parameterisation while maintaining physical relevance. Although the equivalent circuit analysis provides valuable insight, additional characterization, such as XPS, in situ FTIR, or Raman spectroscopy, will be recommended in future studies to verify the formation and evolution of the oxide-like layer observed in this study. A quick comparison of all these fitted parameters is provided in the following sections to understand the role of the FL-Cr_2CT_x-PANI/EP composite in corrosion protection.

Fig. 7A and Table S. 2 show the coating resistance (R_c) of bare steel, neat epoxy, and the FL-Cr_2CT_x-PANI/EP on days 0, 3,5, 7, 14, 21, 30, 50, and 60. Bare steel is not expected to exhibit coating resistance, as it has no coating on its surface. As such, R_c is essentially 0 Ω.cm^2, and the electrolyte reaches the metal surface freely without protection. Neat epoxy has an R_c of ≈approximately 1.09×10^5 Ω.cm^2 at Day 0, which drops rapidly after 3 days of immersion to below 1.5×10^4 Ω.cm^2, a value that is maintained for the remainder of the immersion period. This trend has been reported for unmodified epoxy coating exposed to saline or seawater conditions, where water uptake results in higher ionic conductivity of the medium inside the coating, effectively lowering the R_c [22–24]. The FL-Cr_2CT_x-PANI/EP epoxy coating shows much higher values of R_c that start at 4.23×10^7 Ω.cm^2 on Day 0 and maintain their value above 10^5 Ω.cm^2 until Day 60. This demonstrates the barrier performance of the nanosheets, as well as PANI in the composite, in limiting the permeability of water or ions into the bulk, thereby effectively increasing the tortuosity and potentially incorporating the possible redox activity of PANI at the polymer-metal interface. Barrier performance in epoxy films similarly modified with MXene nanosheets has been reported earlier [5–9].

Charge transfer resistance (R_{ct}) at the metal interface is plotted in Fig. 7B for all three systems. Bare steel is expected to show low R_{ct} values, typically 10^2–10^3 Ω.cm^2, since corrosion is uninhibited in this case in the saline medium. Neat epoxy did not yield any separable R_{ct} values at any time point, which could be due to either the overlapping time constants or limited capacitive behaviour in thin epoxy films without corrosion inhibitors [25,26]. The FL-Cr_2CT_x-PANI/EP coating shows high R_{ct} values that peaked on Day 7 at 2.92×10^6 Ω.cm^2 and remain above 10^5 Ω.cm^2 until Day 60, indicative of charge transfer reactions at the metal interface being suppressed by either the PANI passivating layer or oxidation resistance of FL-Cr_2CT_x.

The constant phase element (CPE) is associated with the coating capacitance (Q_c) and the double layer capacitance (Q_{dl}) in the bare steel case, which is a measure of dielectric behaviour and water uptake at the coating in general. The CPE was converted into a capacitance (Q_x) using Brug's formula (Eq.5) for a more physical interpretation of CPE values in terms of coating capacitance or double-layer capacitance. The trend in Fig. 7D for bare steel shows a slight increase in Q_{dl} from 7.76×10^{-4} to 1.63×10^{-3} F.cm^{-2} by the end of 60 days. This increase can be attributed to the progressive corrosion of the steel surface, which results in the formation of rust products and enhanced surface roughness. As corrosion advances, the effective electrochemically active area exposed to the electrolyte increases, thereby facilitating greater charge accumulation at the metal-solution interface and leading to higher Q_{dl} values [27]. The neat epoxy exhibited Q_c values decreasing from ~10^{-5} to ~10^{-9} F.cm^{-2} between Day 0 and Day 3, followed by stabilization at ~10^{-9} F.cm^{-2} up to 60 days. This behaviour is consistent with reported capacitance values for intact epoxy coatings, where initial water uptake increases the dielectric constant, but subsequent saturation and binding of water molecules lead to stabilization or a decrease in capacitance [25]. FL-Cr_2CT_x-PANI/EP epoxy shows much lower Q_c values in the range of 10^{-10} to 10^{-7} F.cm^{-2}, with transient spikes on Days 7 and 30, which could be attributed to swelling or local interfacial rearrangements. Overall, the lower capacitance across a significant part of the immersion period suggests effective dielectric performance and lower water uptake in the coating as well, which has been observed in other systems that used MXene-modified films as well [5].

The second constant phase element (CPE2) was associated with the double-layer capacitance (Q_{dl}) at the metal/coating interface, shown in Fig. 7D, which provides a quantitative measure of electrochemical activity at the substrate. Neat epoxy did not exhibit a distinguishable Q_{dl}, consistent with the absence of a separate interfacial time constant. In contrast, the FL-Cr_2CT_x-PANI/EP composite coating maintained very low Q_{dl} values in the range of 10^{-10} to 10^{-6} F.cm^{-2}, indicating a highly suppressed electrochemical response at the interface and strongly inhibited corrosion processes throughout the entire immersion period, which is outstanding performance for only a 10 ± 2 μm coating thickness.

Of note, the FL-Cr_2CT_x-PANI/EP system was one of the few cases where a third arc appeared in the Nyquist plot (on Day 7), necessitating the use of an additional time constant to model the capacitance (Q_{ox}) and resistance (R_{ox}) of an oxide-like layer. As shown in Fig. S1A and B, the modelled values of R_{ox} (1.6×10^6 Ω.cm^2) and Q_{ox} (3.10×10^{-10} F.cm^{-2}) suggest the development of a compact, highly resistive oxide film on the steel surface. This oxide may have been chromium oxide (Cr_2O_3), possibly influenced or modified by the PANI phase, and may have acted as a secondary barrier layer; however, this interpretation requires further verification through complementary surface analyses in future work. Similar oxide development phenomena have been reported in MXene-based systems, where a self-limiting oxidation process results in stable oxide barriers that enhance corrosion protection [5]. In contrast, such features were not observed for neat epoxy or bare steel, where corrosion progressed uninhibited.

At the 14-day immersion point, a significant change in the FL-Cr_2CT_x-PANI/EP impedance data was the emergence of a Warburg impedance ($\sigma = 1.67 \times 10^4$ Ω.s$^{-1/2}$.cm^2), as it was modelled with R(Q[RW]) circuit (Table S.1). The Warburg term at the intermediate time points suggests that, after initial electrolyte penetration, corrosion became a diffusion-limited reaction rather than an activation-controlled one. On the other hand, the loss of the Warburg elements after Day 14 and the return to a two-time-constant model suggest that coating was able to re-establish its barrier and passivating properties, either by redox re-stabilization or a second stage of oxide formation. This proposed mechanism should be further examined in future work. In contrast, neat epoxy displayed Warburg behaviour from the early stages of immersion (Day 3), indicative of steady state diffusion through the matrix due to the lack of barrier reinforcement (Fig. 7E). The bare steel system was never modelled with Warburg impedance because the corrosion was activation-controlled at all stages. The evolution of the fitted parameters (R_c, R_{ct}, Q_c, Q_{dl}, R_{ox}, Q_{ox}, W) over immersion time demonstrates that the FL-Cr_2CT_x-PANI/EP epoxy coating delivered multi-layered corrosion protection. Initially, protection was dominated by a strong dielectric barrier (R_c, Q_c), followed by interfacial stabilization (R_{ct}, Q_{dl}). At intermediate immersion stages, a temporary contribution from passive oxide formation (R_{ox}, Q_{ox}) and a transient diffusion-controlled regime (Warburg element, W) were observed. Beyond this stage, the coating re-established long-term impedance stability, suggesting barrier

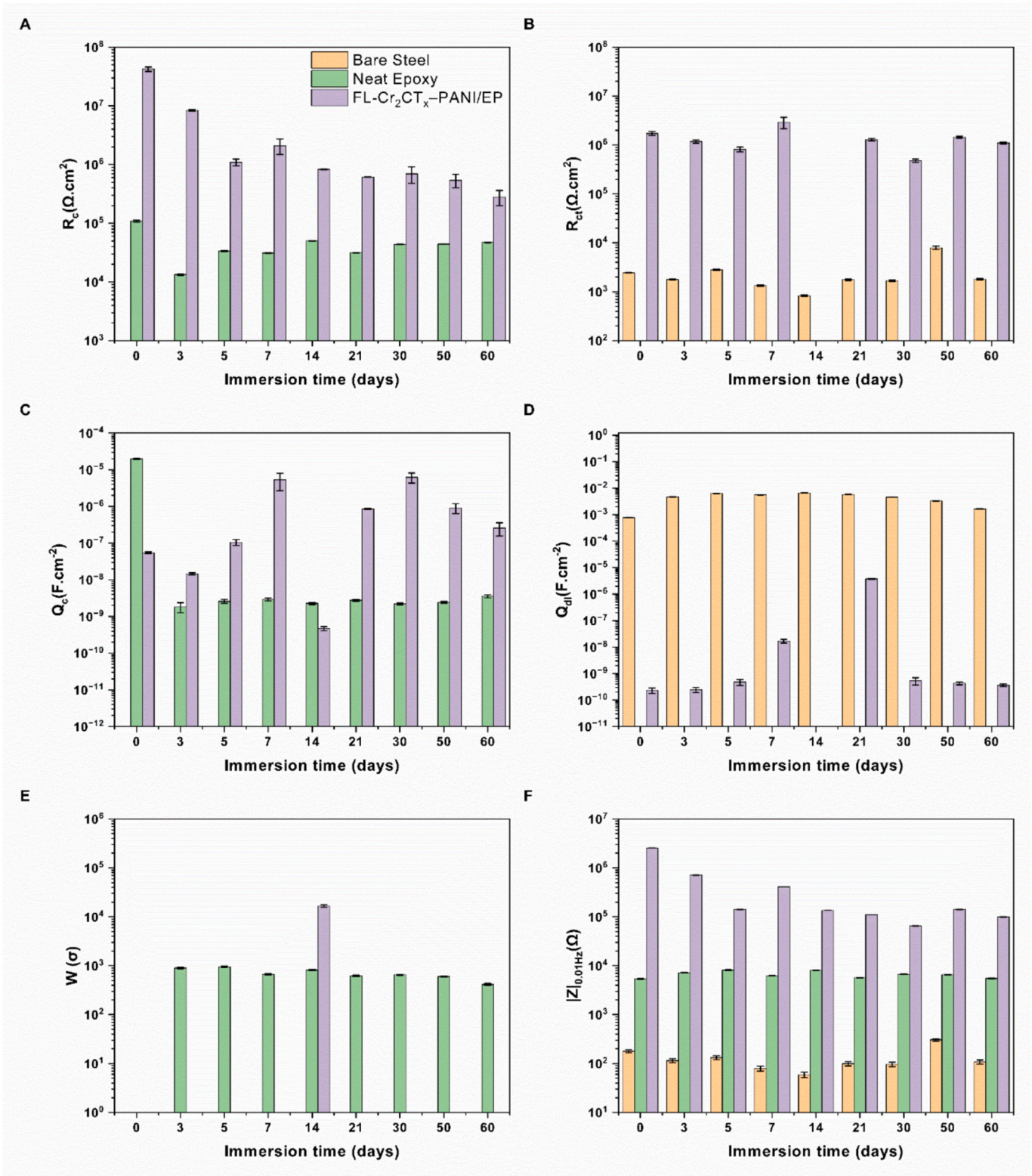

Fig. 7. Equivalent circuit fitting parameters and models derived from EIS analysis of bare steel, neat epoxy, and 0.5 wt% Cr_2CTx + 0.3 wt% PANI/epoxy coatings during 60 days immersion in 3.5 wt% NaCl solution: (A) Coating resistance (R_c) values, showing the FL-Cr_2CT_x-PANI/EP consistently exhibited the highest barrier resistance, (B) Charge transfer resistance (R_{ct}), with the composite coating maintaining superior interfacial resistance, (C) Coating capacitance (Q_c), and (D) double-layer capacitance (Q_{dl}), (E) Warburg impedance (W), highlighting diffusion-controlled behaviour observed for neat epoxy, but minimized in the hybrid coating, (F) the EIS impedance of the various systems at 0.01 Hz.

reinforcement. In contrast, neat epoxy exhibited early dielectric breakdown (Q_c), steady-state diffusion (persistent W), and no passivating contribution, while bare steel underwent continuous activation-controlled corrosion with no sign of impedance recovery. Taken together, these results validate the proposed multi-mechanism corrosion protection model for FL-Cr_2CT_x- PANI/EP coating, in agreement with previous reports on conductive polymer/MXene hybrid systems [6–9].

3.3.2. Structural changes in the composite coating

In order to better understand the changes in the prepared composite coating after the immersion test, the sample that underwent 60 days of testing was analyzed by FTIR and compared with the original sample, as shown in Fig. 8. Following immersion, the general decrease in peak intensity observed across the spectrum, including the bands associated with PANI (the quinonoid/benzenoid rings near 1500 cm^{-1}), is characteristic of moisture-induced swelling and plasticization of the polymer matrix, which decreases the effective concentration of functional groups within the sampled region. Such global intensity loss is typical for epoxy systems after long-term water uptake.

After immersion, the hybrid composite showed broadening and a downshift of the C-O-related peak around 950 cm^{-1} and shifts in the 400–500 cm^{-1} region. These changes are consistent with increased hydrogen bonding as well as the formation/modification of metal-oxide interfacial species on FL-Cr_2CT_x. Low-wavenumber shifts of this type are suggestive of surface terminations toward mixed -O/-OH states during exposure to aqueous media, consistent with the immersion test [28]. In addition, the changes in intensity and wavenumber of the PANI-related band near 1500 cm^{-1} suggest changes in oxidation/protonation state of PANI, caused by interaction with the MXene surface and the immersion environment. This behaviour is attributed to the sensitivity of PANI to local redox and pH conditions [29].

As shown in Fig. S3, the neat epoxy sample similarly shows loss and broadening of epoxide- and ether-related bands (830–1250 cm^{-1}), consistent with epoxide ring opening and increased water uptake. These structural changes were more pronounced in neat epoxy than in the composite. The milder changes in the composite imply reduced water mobility and partial suppression of hydrolytic degradation due to the presence of the FL-Cr_2CT_x-PANI network.

Overall, the FTIR results after immersion indicate that while both systems undergo moisture-related changes, the composite additionally displays MXene- and PANI-derived spectral shifts that support interfacial metal-oxide formation and PANI protonation changes. Together, these features are consistent with a barrier mechanism in which the hybrid filler network limits water access and moderates chemical degradation of the epoxy matrix.

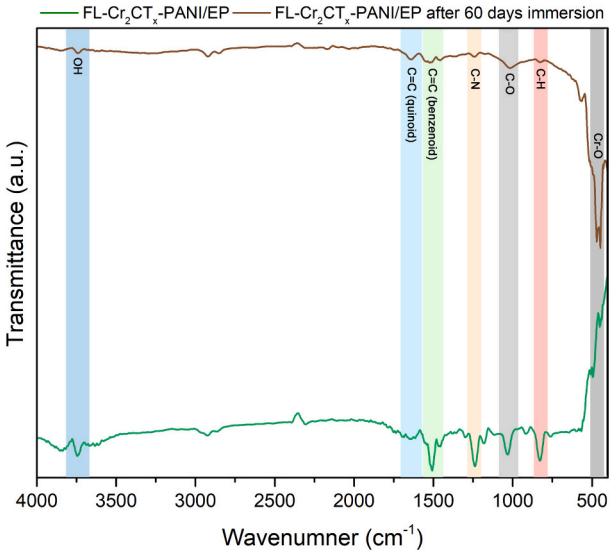

Fig. 8. FTIR spectra of Cr2C-PANI/EP composite pre- and post-immersion test.

3.3.3. Comparative analysis of anticorrosion properties

The protection efficiency of the different MXene-epoxy composites was compared with that of the FL-Cr_2CT_x-PANI/EP composite (Table 2). Most studies in the literature reported coating thicknesses in the range of 20 μm to 100 μm. The only study with a comparable film thickness (13 μm) is the IL@MXene/WEP system, which reported an efficiency of 99.83 % at 10 days. The results of that study and the results presented here confirm the importance of the filler chemistry in MXene composites, as the ionic-liquid modification significantly improved the dispersion, interfacial adhesion, and passivation capability of Ti_3C_2 (IL@MXene) in the WEP matrix [30]. In the study by Zhang et al., the sulfonated PANI-Ti_3C_2 MXene-Zn hybrid (MXP-Zn/EP) composite exhibited only 63.17 % efficiency after 1 day [6]. The poor performance of the MXP-Zn/EP barrier was related to the microporous morphology and galvanic activity of Zn, which together reduced the coating stability. However, the short exposure time questions the long-term performance of that system. The Ti_3C_2 MXene@PANI waterborne epoxy composite described by Li et al. (2022) showed a protection level of 99.71 % at 100 μm and provides evidence for the synergistic effect of the redox-passivating PANI and the dense, well-dispersed MXene sheets. Other hybrids that showed moderate efficiency (e.g., ~76.7 % at 120 μm after 4 days for SMXCGZ/EP) can likely be improved by a more targeted optimization of filler-matrix interactions [31].

The Cr_2CT_x/epoxy coatings reported in the literature showed higher efficiency than the Ti_3C_2 MXene-based composites. For example, the Cr_2CT_x/epoxy coating at a filler loading of 0.5 wt% without PANI showed 94.78 % efficiency after 60 days with a coating thickness of 115 μm [5]. In contrast, the present FL-Cr_2CT_x-PANI/EP system exhibits superior stability for 60 days and at a thickness of only ~10 μm, suggesting that the combined effects of Cr_2C MXene chemistry and the conductive PANI network significantly improve the barrier and passivation capabilities of the epoxy matrix. The synergistic interaction between the conductive fillers is believed to drive redox reactions for re-passivation at defect sites and to reduce the ionic permeability of the coating, which enables long-term protection at low film thickness.

Incorporating 0.3 wt% PANI with FL-Cr_2CT_x filler at an ultra-thin 10 ± 2 μm coating gave 99.85 % and 96.58 % efficiency vs. bare steel and neat epoxy after 60 days, suggesting that, at a significantly lower coating thickness, FL-Cr_2CT_x could provide the same or better long-term efficiency than Ti_3C_2 MXene. This effect is attributed to the PANI polymer, which enhances the dispersion of FL-Cr_2CT_x sheets in the epoxy and provides additional passivation at the metal-coating interface. In contrast to most Ti_3C_2-based systems, which were evaluated at short immersion times (≤10 days), the chromium-based MXene-PANI hybrid maintained a high efficiency after 60 days, demonstrating superior durability. Notably, the FL-Cr_2CT_x disperses more uniformly than the ML-Cr_2CT_x in the epoxy, establishing a denser and more tortuous path that slows down the dispersion of corrosion ions. In addition, the FL-

Table 2
Comparative study of MXene-based epoxy coatings and their anticorrosive efficiencies.

Coating System	Immersion Time (days)	Thickness (μm)	η_{EIS} or η_{PP}^{*} (%)	Ref.
IL@$MXene_{0.5}$/WEP	10	13 ± 1	99.83*	[30]
MXP-Zn/EP	1	–	63.17	[6]
$1.0_{wt\%}$M@P-1.0/WEP	10	100 ± 5	99.71*	[9]
SMXCGZ/EP	4	120	76.73	[31]
0.5 $_{wt\%}$ Cr_2CTx/EP	60	115	94.78 $^{vs.\ EP}$	[5]
$0.5_{wt\%}$FL-Cr_2CT_x-0.3 $_{wt\%}$PANI/EP	60	10 ± 2	99.85$^{vs.\ bare\ steel}$ - 96.58$^{vs.\ EP}$	This study

Cr_2CT_x improves the mechanical integrity of the coating and hence prevents crack propagation that could expose metal.

Nevertheless, from a processing and scalability point of view, the FL-Cr_2CT_x-PANI/EP coating was prepared by a simple solvent-assisted dispersion method and at a low filler loading (0.5 wt% % Cr_2C and 0.3 wt% % PANI) compared to the multi-step vacuum-filtration or layer-by-layer approaches commonly used for $Ti_3C_2T_x$-based coatings. However, the higher oxidation resistance and superior long-term stability make this material more cost-effective for high-value or extended-service applications [5]. A techno-economic and environmental assessment of the industrial feasibility of Cr_2CT_x MXene production and integration in epoxy systems should be the subject of future work.

4. Conclusion

In this study, the fabrication and long-term corrosion protection evaluation of an ultra-thin Cr_2CT_x-PANI/epoxy nanocomposite coating for carbon steel are reported. The XRD, FTIR, and SEM/EDS analyses demonstrated an efficient dispersion of the O-terminated few-layer Cr_2C and strong interfacial interactions with PANI/epoxy to achieve dense, uniform, and well-adherent epoxy films. The hybrid system also possessed high hydrophobicity (contact angle ~106°) and long-term corrosion protection capability with the maintenance of its dense morphology and high contact angle despite its low thickness, different from the cracking and blistering of neat epoxy and the massive pitting corrosion of bare steel.

Electrochemical characterization of the as-fabricated coating systems was performed to understand their corrosion protection mechanisms and revealed that the FL-Cr_2CT_x-PANI/EP hybrid system exhibited the most stable OCP, the lowest corrosion current density, and consistently higher coating and charge transfer resistances than those of neat epoxy and bare steel. The EIS data were successfully fitted to an equivalent circuit model and suggested a multi-mechanistic protection process of the FL-Cr_2CT_x-PANI/EP coating, including the dielectric barrier effect, interfacial stabilization, temporary diffusion-limited behaviour, and the re-establishment of impedance stability, indicating a degree of interfacial stabilization during prolonged immersion. The neat epoxy and bare steel systems, however, displayed early dielectric breakdown and prolonged diffusion-controlled corrosion, and continuous activation-controlled corrosion, respectively. Overall, this study confirms that the addition of 0.5 wt% Cr_2CT_x and 0.3 wt% PANI to epoxy leads to an improvement in the long-term corrosion resistance of the hybrid system by cooperative barrier and passivation mechanisms.

The findings highlight the potential of non-Ti-based MXenes, particularly Cr_2CT_x, as the next-generation nanofillers for advanced, durable, and high-performance anticorrosion coatings, hence broadening the MXene family and offering new opportunities for protection using coatings in aggressive chloride environments. Beyond the performance at the laboratory scale, such ultrathin yet durable coatings can be highly attractive for applications where weight and precision are critical, including aerospace structures, marine engineering components, and microelectronic devices [32]. Additionally, the superior stability of Cr-based MXenes compared to $Ti_3C_2T_x$ further enhances their prospects for industrial use, offering a pathway toward more robust and environmentally stable fillers. Future studies focusing on testing under real marine and industrial conditions will be essential to translate these results into practical protection technologies. Also, techniques such as XPS, Raman spectroscopy, or post-immersion XRD would be valuable for probing chemical state changes of the coating surface that should be examined in future work.

CRediT authorship contribution statement

Abdulmajeed Al Askar: Writing – review & editing, Writing – original draft, Validation, Methodology, Investigation, Formal analysis, Data curation, Conceptualization. **Faris Hamdi:** Writing – review & editing, Formal analysis, Data curation. **Ali Altaee:** Writing – review & editing, Validation, Supervision, Resources, Methodology, Formal analysis, Data curation. **Armaghan Moghaddam:** Writing – review & editing, Validation, Formal analysis, Data curation. **Hossein Ali Khonakdar:** Writing – review & editing, Validation, Formal analysis, Data curation.

Declaration of competing interest

The authors declare that they have no known competing financial interests or personal relationships that could have appeared to influence the work reported in this paper.

Appendix A. Supplementary data

Supplementary data to this article can be found online at https://doi.org/10.1016/j.cej.2025.171884.

Data availability

Data will be made available on request.

References

[1] H. Yan, et al., Amino-functionalized Ti3C2Tx loading ZIF-8 nanocontainer@benzotriazole as multifunctional composite filler towards self-healing epoxy coating, J. Colloid Interface Sci. 602 (2021) 131–145.
[2] M.R.E. Tanjil, et al., Ångström-scale, atomically thin 2D materials for corrosion mitigation and passivation, Coatings (Basel) 9 (2) (2019) 133.
[3] M. Naguib, et al., Two-Dimensional Nanocrystals: Two-Dimensional Nanocrystals Produced by Exfoliation of Ti3AlC2 (Adv. Mater. 37/2011), Adv. Mater. (Weinheim) **23** (37) (2011) 4207.
[4] S. Sharma, A. Kumar, E.E. Ebenso, MXenes and MXene-based nanomaterials for corrosion protection, Mater. Lett. 335 (2023) 133789.
[5] Y. Ning, et al., Oxidation control preparation of chromium-based MXene as ultrahigh performance barrier nanosheets for corrosion protection, Corros. Sci. 235 (2024) 112184.
[6] M. AhadiParsa, A. Dehghani, B. Ramezanzadeh, Sulfonated polyaniline-grafted two-dimensional Ti3C2-MXene (SPANI-MXene) Nanoplatform for designing an advanced smart self-healable coating system, ACS Appl. Mater. Interfaces 15 (20) (2023) 24756–24768.
[7] Y. Dong, et al., Effect of MXene@PANI on the self-healing property of shape memory-assisted coating, Synth. Met. 291 (2022) 117162.
[8] C. Kaewsaneha, et al., Hybrid MXene (Ti3C2Tx)/polyaniline nanosheets as additives for enhancing anticorrosion properties of Zn-epoxy coating, Prog. Org. Coat. 173 (2022) 107173.
[9] C. Li, et al., Synthesis of Ti3C2 MXene@PANI composites for excellent anticorrosion performance of waterborne epoxy coating, Prog. Org. Coat. 165 (2022) 106673.
[10] C.-z. Yang, et al., Preparation and XRD analysis of carbon materials used for Li-ion batteries, in: C.-z. Yang, et al. (Eds.), Materials and Working Mechanisms of Secondary Batteries, Springer Nature Singapore, Singapore, 2023, pp. 159–206.
[11] B. Soundiraraju, R. Raghavan, B.K. George, Chromium carbide Nanosheets prepared by selective etching of aluminum from Cr2AlC for hydrazine detection, ACS Appl. Nano Mater. 3 (11) (2020) 11007–11016.
[12] B. Shalini Reghunath, D. Davis, K.R. Sunaja Devi, Synthesis and characterization of Cr2AlC MAX phase for photocatalytic applications, Chemosphere 283 (2021) 131281.
[13] X. Zou, et al., A simple approach to synthesis Cr2CTx MXene for efficient hydrogen evolution reaction, Mater. Today Energy 20 (2021) 100668.
[14] N. Trainor, Survey of Etching Techniques to Produce Cr2C MXene from Cr2AlC, ProQuest Dissertations & Theses, 2019.
[15] O. Akinola, et al., Synthesis and characterization of Cr2C MXenes, J. Mater. Res. 36 (10) (2021) 1980–1989.
[16] H. Hu, et al., Solvent-free preparation of bio-based composite coating with improved crystallinity and unique corrosion resistance, Prog. Org. Coat. 179 (2023) 107520.
[17] N. Coniglio, et al., Characterizing water sorption in 100% solids epoxy coatings, Prog. Org. Coat. 76 (9) (2013) 1168–1177.
[18] I. Kada, et al., Physical ageing effect on water uptake and adhesion of epoxy coatings by EIS and the blister test, Electrochim. Acta 454 (2023) 142381.
[19] S. Effendy, et al., Blistering failure of elastic coatings with applications to corrosion resistance, Soft Matter 17 (41) (2021) 948–9498.
[20] H. Cao, Beyond graphene and boron nitride: why MXene can be used in composite for corrosion protection on metals? Compos. Part B 271 (2024) 111168.
[21] Z. Nazarlou, et al., Ti3C2 MXene/polyaniline/montmorillonite nanostructures toward solvent-free powder coatings with enhanced corrosion resistance and mechanical properties, ACS Appl. Nano Mater. 6 (10) (2023) 8804–8818.

[22] M. Cai, et al., In Situ Assemble Ti3C2Tx MXene@MgAl-LDH Heterostructure towards Anticorrosion and Antiwear Application, Chem. Eng. J. (Lausanne, Switzerland : 1996) 419 (2021) 130050.
[23] J. Ding, H. Zhao, H. Yu, Structure and performance insights in carbon dots-functionalized MXene-epoxy ultrathin anticorrosion coatings, Chem. Eng. J. (Lausanne, Switzerland : 1996) 430 (2022) 132838.
[24] X. Li, S. Zhou, Dopamine monomer functionalized Ti3C2 nanosheets and their anticorrosion improvement for waterborne epoxy coatings, J. Mater. Res. Technol. 20 (2022) 210–220.
[25] A. Amirudin, D. Thieny, Application of electrochemical impedance spectroscopy to study the degradation of polymer-coated metals, Elsevier B.V, Lausanne, 1995, pp. 1–28.
[26] D.I. Njoku, et al., Understanding the anticorrosive protective mechanisms of modified epoxy coatings with improved barrier, active and self-healing functionalities: EIS and spectroscopic techniques, Sci. Rep. 7 (1) (2017), 15597–15.
[27] P. Kumar, A.N. Shetty, Corrosion behaviour of 18%Ni M250 grade Maraging steel under welded condition in hydrochloric acid medium, Port. Electrochim. Acta 31 (1) (2013) 21–32.
[28] K. Baruah, P. Deb, Enabling methanol oxidation by an interacting hybrid nanosystem of spinel co 3 O 4 nanoparticle decorated MXenes, Dalton Trans. 51 (11) (2022) 4324–4337.
[29] A. Wiorek, et al., Polyaniline films as electrochemical-proton pump for acidification of thin layer samples, Anal. Chem. 91 (23) (2019) 14951–14959.
[30] H. Zhao, et al., Air-stable titanium carbide MXene Nanosheets for corrosion protection, ACS Appl. Nano Mater. 4 (3) (2021) 3075–3086.
[31] P. Najmi, et al., Porous 2D Ti3C2 MXene Nanosheets Sandwiched between Imine-Based Covalent Organic Frameworks (COFs) for Excellent Corrosion Protective Coatings, Chem. Eng. J. (Lausanne, Switzerland : 1996) 456 (2023) 141001.
[32] J.M. Yelwa, et al., Corrosion-resistant coatings: advances in deposition methods, nanostructures, and self-healing films, Acad. Mater. Sci. 2 (3) (2025).